Ingeniería y Competitividad
Vol 26 (3) 2024; doi: 10.25100/iyc.v26i3.13493

Vol 26 (3)

ISSN
0123-3033
e- 2027-8284

Original Article

Fourier analysis for detecting vegetation in hyperspectral images

Análisis de Fourier para la detección de vegetación en imágenes hiperespectrales

Gabriel E. Chanchí-Golondrino[1] Manuel A. Ospina-Alarcón[1] Manuel Saba[1]

[1]Universidad de Cartagena, Facultad de Ingeniería, Cartagena de Indias, Colombia

Abstract

Introduction: hyperspectral images, unlike conventional images, are composed of numerous channels that provide detailed information about the spectral signatures of objects. This allows for the identification of the materials that make them up, and given their potential for detecting environmental changes, identifying vegetation in urban settings using effective computational methods becomes relevant.
Objective: the objective of this research is to propose a computational method based on Fourier analysis for detecting vegetation in hyperspectral images.
Methods: the research was developed in four methodological phases: selection of technologies, acquisition of the characteristic vegetation pixel, determination of phase similarity between the characteristic pixel and vegetation and non-vegetation pixels, validation of the method on a test hyperspectral image. A method was implemented using the spectral and numpy libraries in Python.
Results: the Fourier analysis yielded an average phase similarity of 89.89% and a minimum similarity of 64.54% between the characteristic vegetation pixel and 100 training vegetation pixels. For non-vegetation pixels, the average phase similarity was 42.19%, with a maximum similarity of 63.98%. These results indicate that the proposed method successfully differentiates between vegetation and non-vegetation pixels.
Conclusion: the results demonstrate that the Fourier-based method can accurately identify vegetation areas in hyperspectral images, showing non-overlapping phase similarities between vegetation and non-vegetation. This validates the effectiveness of the proposed approach in detecting vegetation in urban environments.

Keywords: computer vision, fourier analysis, hyperspectral imaging, vegetation detection, remote sensing.

Resumen

Introducción: las imágenes hiperespectrales, a diferencia de las imágenes convencionales, están compuestas por numerosos canales que proporcionan información detallada sobre las firmas espectrales de los objetos. Esto permite identificar los materiales que los componen y, dada su potencialidad en la detección de cambios ambientales, se vuelve relevante la identificación de vegetación en entornos urbanos mediante métodos computacionales eficaces.
Objetivo: el objetivo de esta investigación es proponer un método computacional basado en análisis de Fourier para la detección de vegetación en imágenes hiperespectrales.
Metodología: la investigación se desarrolló en cuatro fases metodológicas: selección de tecnologías, obtención del píxel característico de vegetación, determinación de la similitud de fase entre el píxel característico y los píxeles de vegetación y no vegetación, validación del método en una imagen hiperespectral de prueba. Se implementó un método utilizando las librerías spectral y numpy de Python.
Resultados: el análisis de Fourier obtuvo una similitud de fase promedio de 89.89% y una similitud mínima de 64.54% entre el píxel característico de vegetación y 100 píxeles de vegetación de entrenamiento. Para los píxeles de no vegetación, la similitud de fase promedio fue de 42.19%, con una similitud máxima de 63.98%. Estos resultados indican que el método propuesto logra diferenciar adecuadamente entre píxeles de vegetación y no vegetación.
Conclusiones: los resultados demuestran que el método basado en análisis de Fourier puede identificar con precisión las zonas de vegetación en imágenes hiperespectrales, mostrando similitudes de fase que no se superponen entre vegetación y no vegetación. Esto valida la eficacia del enfoque propuesto en la detección de vegetación en entornos urbanos.

Palabras clave: análisis de Fourier, detección de vegetación, imágenes hiperespectrales, visión por computador, sensado remoto.

How to cite?

Chanchí-Golondrino, G.E., Ospina-Alarcón, M.A., Saba, M. Fourier analysis for detecting vegetation in hyperspectral images. Ingeniería y Competitividad, 2024, 26(3)e-21013493

https://doi.org/10.25100/iyc.v26i3.13493

Recibido: 12-01-24
Evaluado: 30-04-24
Aceptado: 21-06-24
Online: 8-10-24

Correspondence
gchanchig@unicartagena.edu.co

Why was it conducted?
Unlike conventional images, hyperspectral images are composed of numerous channels or bands, which provide detailed information about the spectral signatures of the objects in the images, allowing for the identification of the materials they are composed of. In this context, one of the key challenges is the identification and evaluation of new computational methods different from conventional ones, which enable the detection of materials such as vegetation. Thus, in this article, the use of Fourier phase similarity was proposed for the detection of vegetation spectral signatures in hyperspectral images.**What were**

The most relevant results?
using open-source libraries, the Fourier similarity method was implemented and evaluated with sample pixels of vegetation and non-vegetation. When operating the characteristic vegetation pixel with the vegetation sample pixels, an average similarity of 89.89% and a minimum phase similarity of 64.54% were obtained. Similarly, when operating the characteristic pixel with non-vegetation pixels, an average phase similarity of 42.19% and a maximum phase similarity of 63.98% were obtained. The results demonstrate that the proposed method effectively distinguishes between vegetation and non-vegetation pixels, with phase similarities in both cases that do not overlap.

What do these results contribute?
The results obtained allowed the identification of the Fourier phase similarity method as a viable alternative to traditional material identification methods, such as those based on correlation and machine learning, providing potentially better computational performance than the latter. Thus, this work can be extrapolated to the evaluation of the method's effectiveness in detecting different materials.

Graphical Abstract

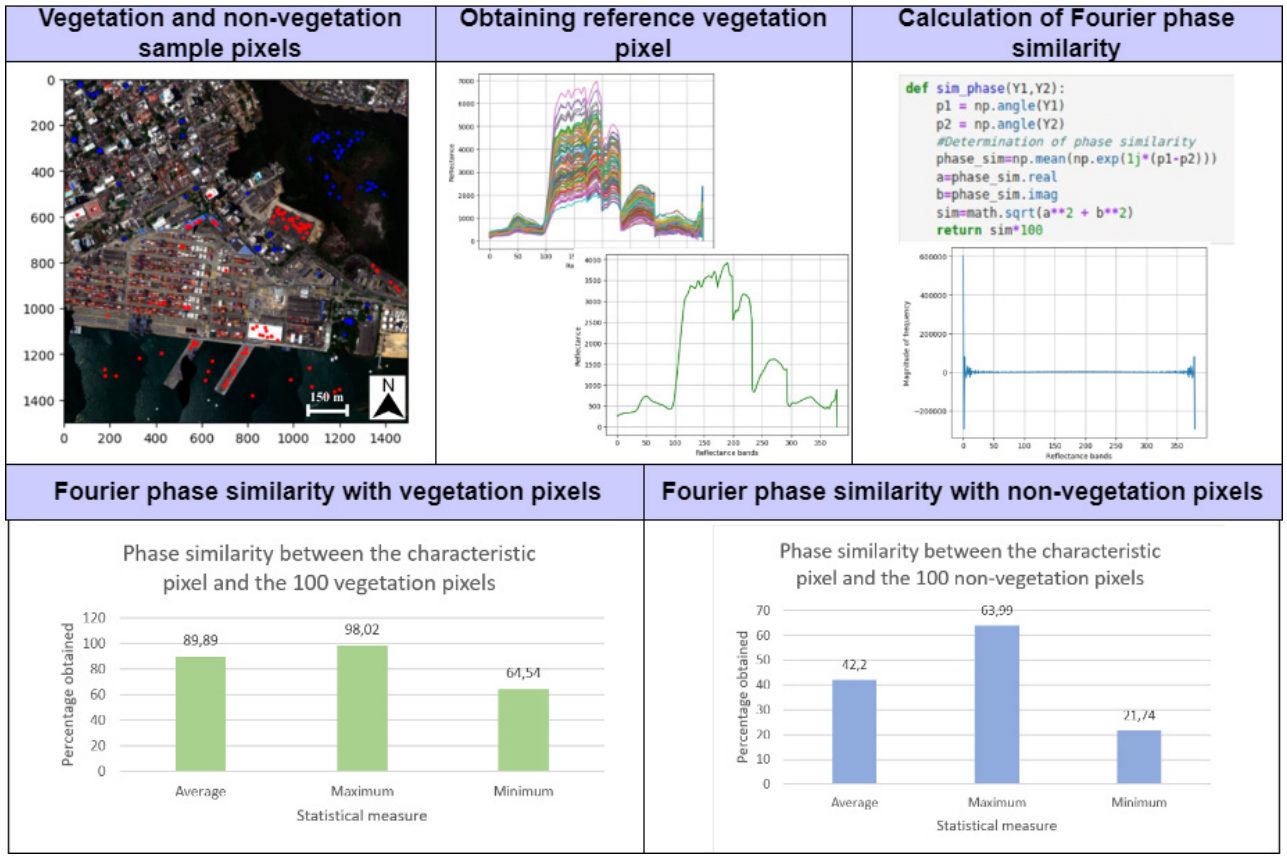

doi: 10.25100/iyc.v26i3.13493

Introduction

For the consolidation of a rational urban environment with respect to the environment and sustainable agriculture, it is crucial to possess greater knowledge about vegetation, soils, crops, forests, water, and other relevant resources. This involves harnessing state-of-the-art technology for the detection and classification of materials, exemplified by hyperspectral imaging (1,2). Hyperspectral images are acquired through the application of remote sensing (RS) techniques, wherein aerial sensors are utilized to capture spatial, temporal, and spectral information of a material or object without physical contact (at the surface, in the atmosphere, and in oceans). This is achieved through the utilization of propagated signals, such as electromagnetic radiation (3,4).

A hyperspectral image is one that encompasses multiple bands of spectral information across the entire electromagnetic spectrum, enabling the detection of elements of interest or objects through the comparison of spectral curves or signatures derived from different bands within the image (5). Specifically, hyperspectral images focus on the solar reflectance region spanning from 400 nm to 2500 nm, covering the visible spectrum (VIS), visible infrared (NIR), and shortwave infrared (SWIR) (6,7). In the context of hyperspectral images, data structures known as hypercubes or data cubes (3D images) are generated, obtained by combining spatial dimensions with a third spectral dimension (8–11). The study of hyperspectral images thus facilitates the development of practical solutions that enable understanding, characterization, and modeling of natural resources, as well as fostering the monitoring of their dynamics in both time and space (1).

Hyperspectral images have various applications across different fields, encompassing a broad spectrum of uses (12). These applications range from military surveillance (13), where these images have been utilized to gather detailed information in security contexts, to the detection of pests and diseases in crops (14), enabling early and precise diagnosis. In the field of forest management, these images have been employed in the monitoring and control of forest resources (15). The capability of hyperspectral images to analyze material composition is reflected in their application in determining the fermentation of crop seeds (16) and in the identification and characterization of mineral resources and metals (17). Moreover, these images have also ventured into the astronomical realm, allowing for the determination of the chemical composition of stars (18). Despite the widespread adoption of these techniques, one of the main challenges lies in developing efficient methods for processing the large volumes of information generated by hyperspectral image data cubes. These methods must enable effective material detection based on their spectral signatures (1,9,18–20). In this context, the use of machine learning techniques, particularly supervised learning, requires a sufficient number of samples to train the models (21). Therefore, it is crucial to evaluate and compare various computational approaches that enable the accurate detection of materials in hyperspectral images based on their spectral signatures.

Additionally, these images have applications in environmental monitoring, enabling the observation of changes in terrestrial temperature, oceans, and submarine topography (22,23). Likewise, they are crucial for mapping large-scale forest fires, tracking clouds, and contributing to climate prediction (24). Moreover, they have the capability to observe volcanic eruptions and monitor particulate matter storms (25). Within their extensive range of applications, hyperspectral images are also essential in urban planning, geology, oil and gas exploration, and other areas (26). These images facilitate the monitoring of urban development through multi-temporal analyses, the identification of ground objects such as asbestos-cement roofs, and support humanitarian and planning efforts across various disciplines.

In this same vein, within the vast landscape of hyperspectral image analysis methods, various approaches have stood out, garnering considerable attention in research and application. Among these methods, distance/correlation metrics and machine learning have emerged as widely studied and recognized approaches. Distance/correlation metrics are based on comparing the spectral signatures of different pixels, enabling the evaluation of similarity between them and extracting valuable information about the materials present in the image (27). On the other hand, machine

doi: 10.25100/iyc.v26i3.13493

learning offers the capability to develop sophisticated predictive models from large datasets, allowing for accurate classification and detection of materials and objects (28). However, it is important to note that, within this diverse panorama, there are methods that have not yet received the same level of attention, such as those based on Fourier analysis. Despite their significant potential to decompose spectral signals and reveal hidden patterns, these methods have been relatively less explored compared to distance/correlation metrics and machine learning. This gap in the study highlights an intriguing opportunity to expand the understanding, knowledge, and utilization of the benefits that Fourier analysis-based methods could bring to hyperspectral image analysis.

In this paper, we propose a novel contribution in the form of a new method based on Fourier analysis, specifically utilizing Fourier phase similarity, for the identification and/or detection of vegetation within the context of hyperspectral images. To implement the method, a characteristic pixel associated with the spectral signature of vegetation was obtained, such that the method's accuracy was assessed in comparison to 100 vegetation pixels and 100 non-vegetation pixels, each comprising 380 frequency bands. Following the determination of the efficacy of the proposed method, validation was performed on a hyperspectral image of the Manga neighborhood in Cartagena de Indias, consisting of 1500 x 1500 pixels and 380 bands. The proposed method was implemented using open-source libraries in the Python language, such as spectral, pandas, numpy, and matplotlib. Based on the results obtained with the proposed method, this approach aims to be extrapolated in the academic and research context for the implementation of detection methods for various types of materials within the environmental context, with the goal of facilitating the temporal monitoring of the distribution of these materials in urban context.

The rest of the article is organized as follows: Section 2 presents the different methodological phases employed for the development of the current research. Section 3 describes the results obtained in this study, including the derivation of the characteristic vegetation pixel, the evaluation of the method with a set of test pixels (100 vegetation pixels and 100 non-vegetation pixels), as well as the validation with a hyperspectral image corresponding to the Manga neighborhood in the city of Cartagena de Indias. Finally, Section 4 presents the conclusions and future work derived from this research.

Methodology

Four methodological phases were defined for the development of this research: selection of technologies for the processing and analysis of hyperspectral images, obtaining the characteristic pixel or average pixel, determination of the Fourier phase similarity between the vegetation pixel and the sample pixels (vegetation and non-vegetation), and finally validation of the method on a hyperspectral test image (see Figure 1).

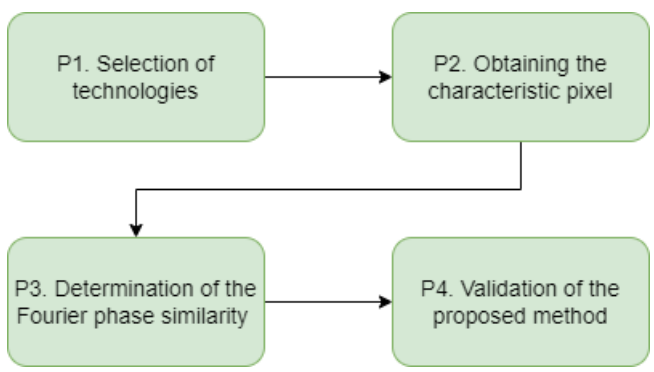

Figure 1. Methodology considered. Source: own elaboration.

doi: 10.25100/iyc.v26i3.13493

In the first phase of the methodology, the spectral library in Python was initially chosen for reading and processing the different bands or layers of the hyperspectral image used in this research. Additionally, the numpy library in Python was selected for obtaining the Fourier transform of each pixel in the image, as well as for calculating the phase similarity between pixels. Moreover, the advantages provided by the matplotlib library in Python were utilized for plotting the different pixels of the hyperspectral image.

In the second phase of the methodology, a set of 100 vegetation pixels and 100 non-vegetation pixels were selected from a test hyperspectral image for the subsequent model evaluation. From the 100 vegetation pixels, the average pixel or characteristic vegetation pixel was derived, representing the spectral signatures of the 100 vegetation pixels. Thus, the characteristic or average pixel consists of an array with 380 positions, each containing the average reflectance of the n-th spectral band from the 100 selected vegetation pixels. This approach is suitable for working with the Fourier transform, as it allows the decomposition of a signal into its frequency components, thereby providing information about the frequency distribution.

In the third phase, based on the characteristic vegetation pixel, the Fourier phase similarity between the characteristic pixel and each of the 100 vegetation and non-vegetation pixels was calculated. This aimed to assess the accuracy of the proposed method and, consequently, its ability to differentiate between vegetation pixels and other pixels. For this purpose, both the characteristic pixel and the other pixels underwent fast Fourier transform using the methods provided by the numpy library. Thus, Equation (1) represents the fast Fourier transform applied to each pixel in the image. The fast Fourier transform can be understood as an algorithmically efficient computational method for calculating the discrete Fourier transform (29).

$$X(k) = \frac{1}{N} \sum_{n=0}^{N-1} x(n) \cdot e^{-j \cdot \frac{2\pi}{N} k \cdot n} \quad (1)$$

Where $x(n)$ represents the spectral signature of the image as a function of band n, k is the phase of the spectrum, and N represents the number of bands in each hyperspectral image. In the same manner, the phase similarity calculated between the Fourier transforms of each pixel is presented in Equation (2).

$$similarity(Y_1, Y_2) = \frac{1}{N} \sum_f e^{j\Delta\phi_f} \times 100 \quad (2)$$

Where Y1 and Y2 correspond to the Fourier transform of the 2 correlated pixels of 380 bands, that is, in this case, Y1 refers to the Fourier transform of the characteristic pixel and Y2 corresponds to the Fourier transform of the evaluated pixel. Similarly, N corresponds to the total number of frequencies in the signals Y_1 and Y_2, while $\Delta\phi_f$ is the phase difference at frequency f, defined in Equation (3) as:

$$\Delta\phi_f = \angle Y_1(f) - = \angle Y_2(f) \quad (3)$$

Similarly, $e^{j\Delta\phi_f}$ represents the complex exponential of the phase difference at frequency f, and $\sum_f$ is the summation over all frequencies. Thus, Equation (2) calculates the similarity between the phases of the two signals at each frequency, and then averages these values across all frequencies (30).

doi: 10.25100/iyc.v26i3.13493

Finally, in the fourth phase of the methodology, and once the proposed method was evaluated, this method was applied to all pixels in a test image of 1500 x 1500 pixels with 380 bands per pixel (see Figure 2), corresponding to the Manga neighborhood in Cartagena. In this way, pixels exceeding a certain similarity threshold with respect to the average or characteristic pixel were highlighted in the image.

Figure 2. Reference hyperspectral image considered in the study. Source: own elaboration.

Results and discussion

As mentioned in the methodology of this study, initially, a sample of 100 vegetation and non-vegetation pixels was taken from the image presented in Figure 2 to assess the accuracy of the Fourier analysis-based method. In Figure 3, the 100 selected vegetation pixels are shown in blue, while the non-vegetation pixels (water, roofs, containers, roads, cars, among others) are presented in red. It is worth noting that, unlike the pixels in a conventional RGB image, which have 3 color channels (red, green, and blue), each pixel in the hyperspectral image considered in this case has a total of 380 spectral bands. These bands form the spectral signature of the materials from which the pixels were sampled. When plotting the reflectance of the 380 bands corresponding to the 100 vegetation pixels, the curve shape is similar because the 380 bands reflect the specific reflectance of vegetation. Conversely, the 100 non-vegetation pixels include the spectral signatures of different materials, as the reflectance values of the 380 bands vary by material. Thus, the 100 spectral signatures of the vegetation pixels provide sufficient information about this material in their 380 bands to be used in vegetation characterization.

doi: 10.25100/iyc.v26i3.13493

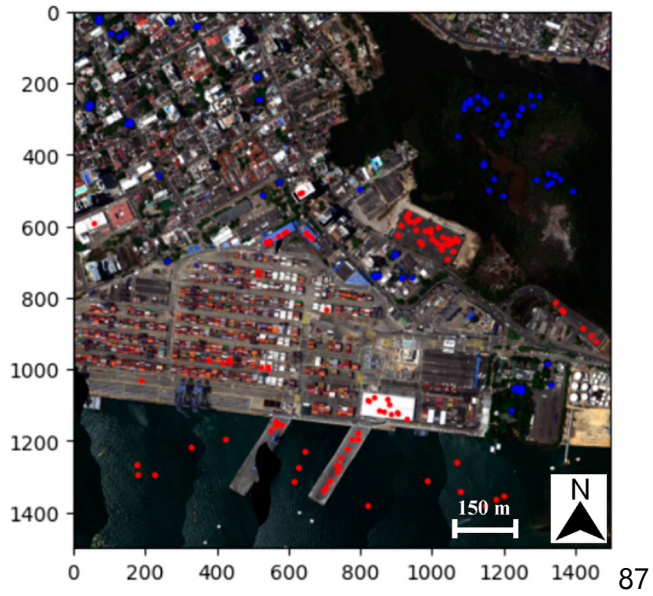

87

Figure 3. Selected sample pixels. Source: own elaboration.

From the 100 sample vegetation pixels, the characteristic pixel of the vegetation spectral signature was obtained by averaging the 100 pixels using the numpy library. Thus, Figure 4 presents both the group of 100 pixels and the characteristic pixel derived from averaging them.

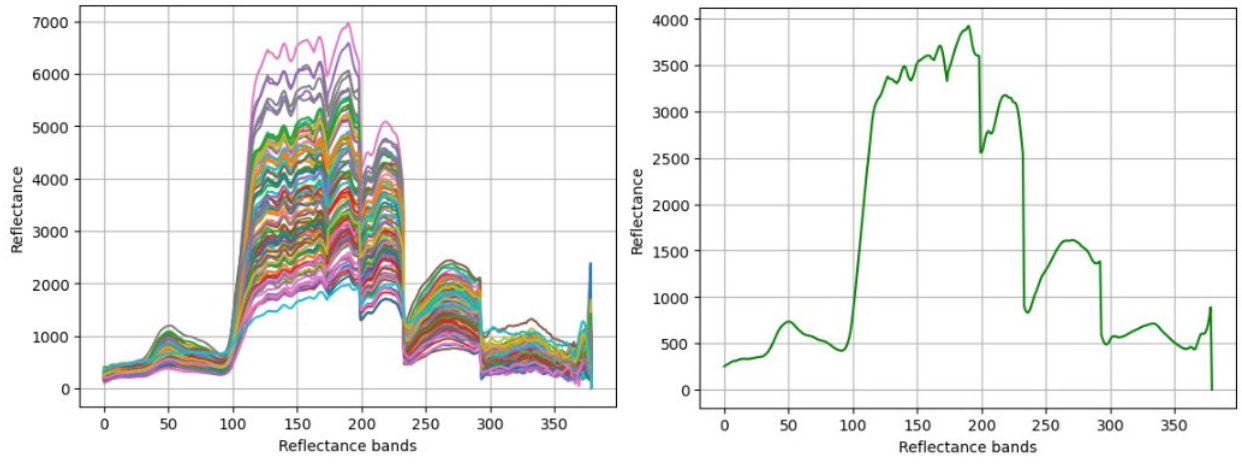

Figure 4. Characteristic pixel of vegetation. Source: own elaboration.

Thus, from Figure 4, it can be observed that the characteristic or average pixel corresponds to an array of 380 positions, where each position represents the average reflectance of the n-th band from 100 vegetation sample pixels. Each sample pixel included in the average has 380 reflectance bands. Using the characteristic pixel from Figure 4, the phase similarity with the 100 vegetation and non-vegetation pixels was obtained by computationally implementing Equations (1), (2), and (3). Thus, Figure 5 illustrates the implementation of a Python function that determines the Fourier phase similarity, taking the fast Fourier transforms of the two pixels to be correlated as parameters. As depicted in Figure 5, the phase similarity was implemented using the functionalities provided by the numpy library in Python.

doi: 10.25100/iyc.v26i3.13493

```python
def sim_phase(Y1,Y2):
    p1 = np.angle(Y1)
    p2 = np.angle(Y2)
    #Determination of phase similarity
    phase_sim=np.mean(np.exp(1j*(p1-p2)))
    a=phase_sim.real
    b=phase_sim.imag
    sim=math.sqrt(a**2 + b**2)
    return sim*100
```

Figure 5. Implementation of the phase similarity function. Source: own elaboration.

On the other hand, in Figure 6, the fast Fourier transform obtained for the case of the average pixel is presented, which is correlated using the algorithm shown in Figure 5 with the different selected pixels. Although from Figure 6 it is possible to observe that the Fourier transform of the characteristic pixel is not centered, it is important to mention that the analysis seeking to determine if a pixel corresponds to vegetation is not performed directly from the transform, but rather from the phase similarity or relative phase between the two pixels.

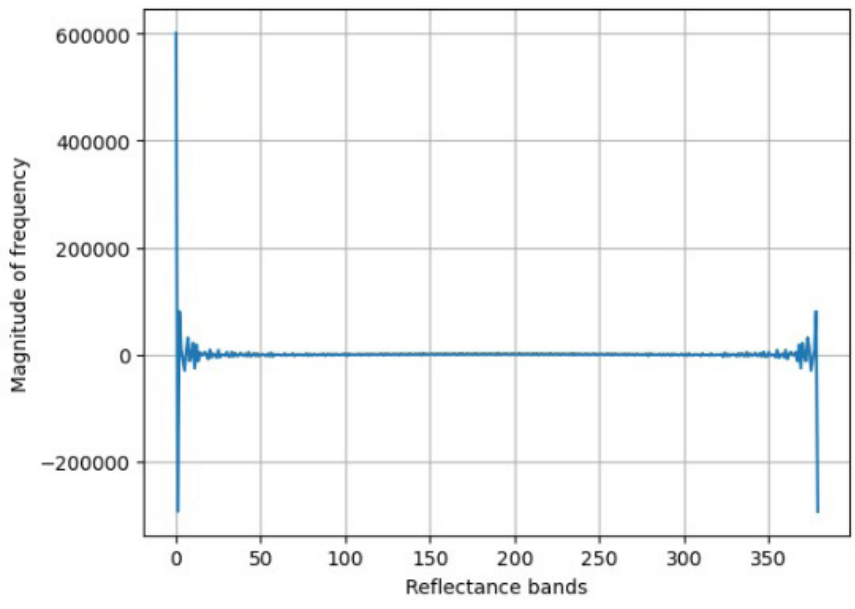

Figure 6. Fast Fourier transform of the characteristic pixel. Source: own elaboration.

When determining the phase similarity between the average or characteristic pixel and each of the 100 vegetation pixels, it is possible to observe in Figure 7 that the average similarity obtained was 89.89%, with a maximum similarity value of 98.02% and a minimum value of 64.54%. Similarly, the standard deviation obtained among the phase similarities was 6.86. Likewise, the minimum threshold that should not be exceeded when analyzing non-vegetation pixels is 64.54%.

doi: 10.25100/iyc.v26i3.13493

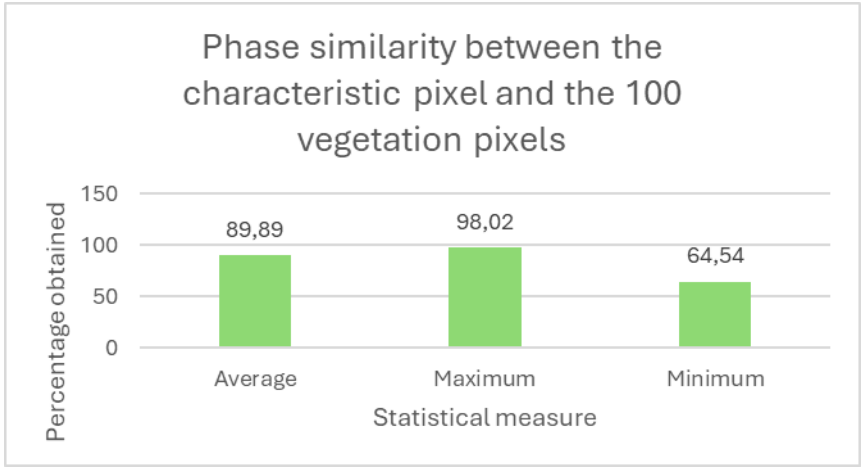

Figure 7. Results obtained with vegetation pixels. Source: own elaboration.

In a similar vein, when calculating the phase similarity between the average or characteristic pixel and each of the 100 non-vegetation pixels, it is possible to observe in Figure 8 that the average similarity obtained was 42.2%, with a maximum similarity value of 63.99% and a minimum value of 21.74%. Similarly, the standard deviation obtained among the phase similarities was 7.15. In the same way, the maximum threshold for non-vegetation pixels, which will be used for comparison with the minimum threshold for vegetation, is set at 63.99%.

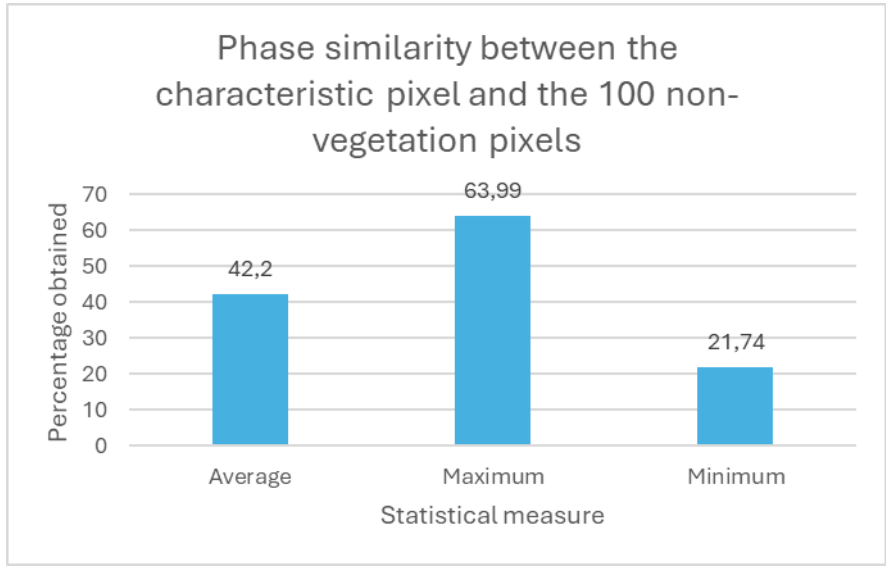

Figure 8. Results obtained with non-vegetation pixels. Source: own elaboration.

When comparing the minimum vegetation threshold (64.54%) with the maximum non-vegetation threshold (63.99%), it is evident that, despite the 0.55% difference between them, these values do not overlap. Therefore, the Fourier analysis-based method, specifically focusing on Fourier phase similarity, can be used for vegetation detection in hyperspectral images, taking the minimum

doi: 10.25100/iyc.v26i3.13493

comparison threshold as 64.54%. In this regard, it is possible to observe that the reflectance values of the 380 bands corresponding to the 100 selected vegetation pixels from the considered hyperspectral image allowed for an adequate characterization of the vegetation's spectral signature. This indicates that the average pixel obtained accurately captured the information on the various changes in the spectral curve across the 380 bands. On the other hand, it is important to mention that although the Fourier transform obtained from vegetation pixels is not centered, the phase similarity between the Fourier transforms of these pixels allows for slight differentiation from pixels of other materials.

After evaluating and comparing the method with vegetation and non-vegetation pixels, the characteristic pixel was then correlated with the 2,250,000 pixels of 380 bands present in the test image corresponding to the Manga neighborhood in Cartagena. Thus, in Figure 9, the algorithm employed for vegetation detection in the hyperspectral image is depicted, using a minimum detection threshold value of 64.54%. Similarly, in Figure 9, the detected vegetation in the test hyperspectral image is presented in blue, applying the implemented method. It can be observed that the visually obtained results align with the vegetation areas shown in Figure 2.

```
Y1=np.fft.fft(pix_prom)
arr_copia=np.copy(arr)

tam=arr.shape
cont_pix=0
for i in range(0, tam[0]):
    for j in range(0, tam[1]):
        arr_temp=arr[i,j,:]
        nz=arr_temp.size - np.count_nonzero(arr_temp)
        if(nz!=380):
            Y2=np.fft.fft(arr_temp)
            sim=sim_phase(Y1,Y2)
            if(sim>64.54):
                arr_copia[i][j]=150
                cont_pix+=1
```

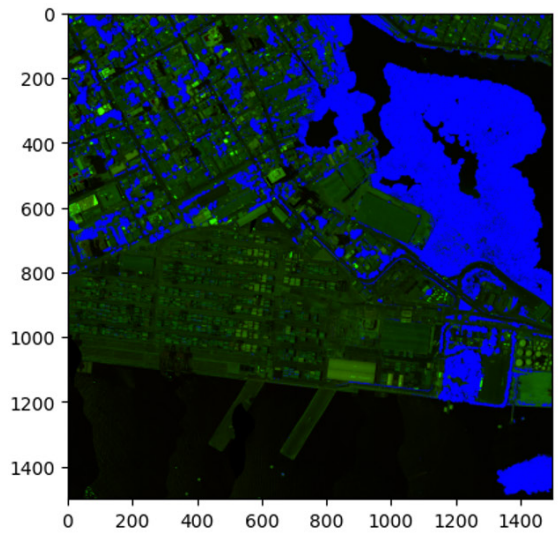

Figure 9. Application of the proposed method on the test hyperspectral image. Source: own elaboration.

Furthermore, upon counting the detected vegetation pixels, it was found that the proposed method identified a total of 452,801 vegetation pixels. This signifies that vegetation pixels account for 20.12% of the total pixels, considering pixels corresponding to various materials. This underscores the relevance of the proposed method in monitoring vegetation or other environmentally significant elements, such as water, over time in the urban sector.

In terms of discussion, it is important to mention that, in comparison to the results obtained in (27), where vegetation detection methods based on distance and/or correlation metrics were evaluated, the proposed method, while obtaining lower average similarity values and lower threshold values, exhibits no overlap between vegetation and non-vegetation pixels. Therefore, the proposed method stands as a valid alternative for vegetation detection in hyperspectral images. Similarly, considering that the application of the fast Fourier transform centers values on specific phases, it is possible that the computation of similarities is more efficient.

On the other hand, regarding the work of (30), where the authors use the fast Fourier transform for detecting water bodies in hyperspectral images, the spectral signature of the water bodies could not be detected when considering all 380 bands. This resulted in overlaps in the phase similarity

doi: 10.25100/iyc.v26i3.13493

percentages between water body pixels and other pixels, necessitating the identification of the most relevant bands where phase similarity could adequately distinguish water bodies. Therefore, it is important to mention that the fast Fourier transform demonstrated suitable accuracy in detecting the characteristic curve of vegetation. However, for other materials, it may be necessary to evaluate and determine the bands where phase similarity does not overlap, considering that the spectral signature of each material is different.

Conclusions

In this paper, a new approach was proposed as a contribution to the identification of vegetation in hyperspectral images. This approach is based on the use of Fourier analysis, specifically focusing on the phase similarity calculated between the characteristic vegetation pixel (average pixel) and the other pixels in a hyperspectral test image. The proposed method aims to serve as a reference at an academic level and for environmental entities in the development of environmental studies, with the goal of identifying the distribution of vegetation in an urban area and monitoring changes in vegetation distribution over time within a city.

It was observed that since different materials exhibit distinct spectral signatures, there is a possibility of phase similarity overlap when addressing all bands in hyperspectral images, as evidenced in the study presented in (30). Hence, it becomes imperative to assess which bands are pertinent for phase similarity to accurately determine the spectral signature of the material. In this context, for the investigation outlined in this paper, which focused on detecting vegetation pixels, it is noteworthy that Fourier phase similarity exhibited no overlap. Thus, the proposed method proves effective in detecting the characteristic vegetation curve using all 380 bands in the image.

While various proprietary tools exist for the analysis and processing of hyperspectral images within the context of geographic information systems, this study demonstrated the utility and significant potential of open-source tools and technologies. To process and access pixels and bands in hyperspectral images, the spectral and pandas libraries of Python were employed. The implementation of the Fourier analysis-based method benefited from the advantages provided by the numpy library in Python. Finally, for pixel visualization and the display of hyperspectral images, the matplotlib and spectral libraries were respectively utilized. Thus, this study aims to serve as a reference regarding the utilization of these tools in the implementation of detection methods on hyperspectral images within academic and research contexts.

The proposed method in this article resulted in an average similarity of 89.99% with vegetation pixels and a 42.2% similarity with non-vegetation pixels (such as water, asbestos, roads, containers, among others). Additionally, the minimum threshold detected with vegetation pixels was 64.54%, while the maximum threshold obtained with non-vegetation pixels was 63.99%. The foregoing results indicated that, although the previous thresholds are close, there was no overlap between them, suggesting that the method can be appropriately employed for the recognition of the spectral signature corresponding to vegetation pixels. Thus, based on the results obtained in this research, the proposed method can be considered as a foundation for the development of software applications focused on the analysis and detection of different types of materials in hyperspectral images, each case considering the spectral signature of the respective materials.

The proof of concept developed using the proposed method allowed determining that in the hyperspectral image of the Manga neighborhood in the city of Cartagena de Indias, approximately 20% of the detected materials correspond to vegetation. This proof of concept verified the relevance of the method and its significant potential as a support for conducting environmental studies focused on monitoring urban changes and their impact on the environment by research centers and government entities. This is achieved by leveraging the advantages provided by open-source software for developing countries, given the high costs of licenses for processing and analyzing hyperspectral images.

doi: 10.25100/iyc.v26i3.13493

As a future work arising from the present research, the following objectives are intended: a) to compare the computational efficiency of the proposed method with respect to methods based on correlation and/or distance metrics; b) to test the effectiveness and efficiency of the computational method by considering the most representative frequency bands, i.e., those in which average pixels of vegetation and non-vegetation exhibit the greatest difference; c) to analyze the effectiveness of the proposed method in detecting other types of materials, such as asbestos or water.

CRediT authorship contribution statement

Manuel Saba: conceptualization, Formal analysis, Investigation, Project administration, Funding acquisition, Resources, Writing – review & editing. Manuel A. Ospina: conceptualization, Data curation, Investigation, Methodology, Supervision, Validation, Writing – review & editing. Gabriel E. Chanchí Golondrino: Data curation, Formal analysis, Methodology, Software, Visualization, Writing – original draft.

Ethical implications

The authors do not have any type of ethical involvement that should be declared in the writing and publication of this article.

Conflict of interest

The autors no declare.

Funding

This article is considered a product within the framework of the project 'Development of a comprehensive strategy to reduce the impact on public health and the environment due to the presence of asbestos in the territory of the department of bolívar,' funded by the General Royalties System of Colombia (SGR) and identified with code BPIN 2020000100366. This project was carried out by the University of Cartagena, Colombia, and the Asbestos-Free Colombia Foundation. Finally, the authors would like to express their gratitude to Federico Frassy for his support in the management and classification of hyperspectral data, to Aiken Hernando Ortega Heredia, María Angélica Narváez Cuadro, Carlos Andrés Castrillón Ortiz, Michelle Cecilia Montero Acosta, Margareth Peña Castro, Carlos David Arroyo Angulo, and the rest of the research team for logistical support and sample collection in the field. Additionally, the authors extend their thanks to Juan Manuel González from BlackSquare company for assistance in acquiring hyperspectral data and to Sean Fitzgerald for the PLM analysis

References

1. León-Pérez J. Imágenes hiperespectrales y sus aplicaciones en estudios de suelos, cultivos y bosques, en la era de la cuarta revolución industrial. Rev UD y la Geomática. 2021;(16):40–70.

2. Erturk A, Cesmeci D, Gullu MK, Gercek D, Erturk S. Endmember Extraction Guided by Anomalies and Homogeneous Regions for Hyperspectral Images. IEEE J Sel Top Appl Earth Obs Remote Sens [Internet]. 2014 Aug;7(8):3630–9. Available from: https://ieeexplore.ieee.org/document/6847728/

3. Richards JA. Remote Sensing Digital Image Analysis [Internet]. Berlin, Heidelberg: Springer Berlin Heidelberg; 2013. Available from: https://link.springer.com/10.1007/978-3-642-30062-2

4. Camacho-Velasco A, Vargas-García CA, Rojas-Morales FA, Castillo-Castelblanco S, Arguello-Fuentes H. Aplicaciones y retos del sensado remoto hiperespectral en la geología colombiana. Rev Fac Ing. 2015;24(40):17–29.

doi: 10.25100/iyc.v26i3.13493

5. Roman-Gonzales A. Análisis de imágenes hiperespectrales. Rev Ing Desarro. 2013;9(35):14–7.

6. Shaw GA, Burke HK. Spectral Imaging for Remote Sensing. Lincoln Lab J. 2003;14(1):3–28.

7. Cerra D, Muller R, Reinartz P. Noise Reduction in Hyperspectral Images Through Spectral Unmixing. IEEE Geosci Remote Sens Lett [Internet]. 2014 Jan;11(1):109–13. Available from: https://ieeexplore.ieee.org/document/6488723/

8. Liu J, Wu Z, Xiao L, Sun J, Yan H. Generalized Tensor Regression for Hyperspectral Image Classification. IEEE Trans Geosci Remote Sens [Internet]. 2020 Feb;58(2):1244–58. Available from: https://ieeexplore.ieee.org/document/8877994/

9. Paoletti ME, Hautt J., Plaza J, Plaza A. Estudio Comparativo de Tecnicas de Clasificación de Imágenes Hiperespectrales. Rev Iberoam Automática e Informática Ind. 2019;(16):129–37.

10. Diezma B, Lleó L, Herrero A, Lunadei L, Roger JM, Ruiz-Altisent M. La imagen hiperespectral como herramienta de evaluación de la calidad de hortaliza de hoja mínimamente procesada. In: VI Congreso Ibérico en Agroingeniería. 2011. p. 1–9.

11. Li J, Li Y, Wang C, Ye X, Heidrich W. BUSIFusion: Blind Unsupervised Single Image Fusion of Hyperspectral and RGB Images. IEEE Trans Comput Imaging [Internet]. 2023;9:94–105. Available from: https://ieeexplore.ieee.org/document/10037221/

12. Fan Y, Ni D, Ma H. HyperDB: a hyperspectral land class database designed for an image processing system. Tsinghua Sci Technol [Internet]. 2017 Feb;22(01):112–8. Available from: http://ieeexplore.ieee.org/document/7830901/

13. Banerjee A, Burlina P, Diehl C. A support vector method for anomaly detection in hyperspectral imagery. IEEE Trans Geosci Remote Sens [Internet]. 2006 Aug;44(8):2282–91. Available from: http://ieeexplore.ieee.org/document/1661816/

14. Bannari A, Pacheco A, Staenz K, McNairn H, Omari K. Estimating and mapping crop residues cover on agricultural lands using hyperspectral and IKONOS data. Remote Sens Environ [Internet]. 2006 Oct;104(4):447–59. Available from: https://linkinghub.elsevier.com/retrieve/pii/S0034425706002148

15. Lawrence RL, Wood SD, Sheley RL. Mapping invasive plants using hyperspectral imagery and Breiman Cutler classifications (randomForest). Remote Sens Environ [Internet]. 2006 Feb;100(3):356–62. Available from: https://linkinghub.elsevier.com/retrieve/pii/S0034425705003792

16. Soto Bohorquez JC, Ruiz Reyes JM, Ipanaque Alama W, Chinguel Alama C. New Hyperspectral Index for Determining the State of Fermentation in the Non-Destructive Analysis for Organic Cocoa Violet. IEEE Lat Am Trans [Internet]. 2018 Sep;16(9):2435–40. Available from: https://ieeexplore.ieee.org/document/8789565/

17. Kokaly RF, Hoefen TM, Graham GE, Kelley KD, Johnson MR, Hubbard BE, et al. Mineral information at micron to kilometer scales: Laboratory, field, and remote sensing imaging spectrometer data from the orange hill porphyry copper deposit, Alaska, USA. In: 2016 IEEE International Geoscience and Remote Sensing Symposium (IGARSS) [Internet]. IEEE; 2016. p. 5418–21. Available from: http://ieeexplore.ieee.org/document/7730411/

18. Fickus M, Lewis ME, Mixon DG, Peterson J. Compressive Hyperspectral Imaging for Stellar Spectroscopy. IEEE Signal Process Lett [Internet]. 2015 Nov;22(11):1829–33. Available from: http://ieeexplore.ieee.org/document/7115943/

19. Della Porta CJ, Chang C-I. Progressive Compressively Sensed Band Processing for Hyperspectral Classification. IEEE Trans Geosci Remote Sens [Internet]. 2021 Mar;59(3):2378–90. Available from: https://ieeexplore.ieee.org/document/9123599/

doi: 10.25100/iyc.v26i3.13493

20. Fen Chen, Ting Feng Tang, Ke Wang. Low-Rank Decomposition Model for Adaptive Identification of Similar Neighboring Pixels in Hyperspectral Images. IEEE Geosci Remote Sens Lett [Internet]. 2016 Feb;13(2):172–6. Available from: http://ieeexplore.ieee.org/document/7360895/

21. Wu Z, Shi L, Li J, Wang Q, Sun L, Wei Z, et al. GPU Parallel Implementation of Spatially Adaptive Hyperspectral Image Classification. IEEE J Sel Top Appl Earth Obs Remote Sens [Internet]. 2018 Apr;11(4):1131–43. Available from: https://ieeexplore.ieee.org/document/8066284/

22. Krug LA, Platt T, Sathyendranath S, Barbosa AB. Ocean surface partitioning strategies using ocean colour remote Sensing: A review. Prog Oceanogr. 2017 Jun;155:41–53.

23. Rani M, Masroor M, Kumar P. Remote sensing of Ocean and Coastal Environment – Overview. In: Remote Sensing of Ocean and Coastal Environments. Elsevier; 2021. p. 1–15.

24. Wetherley EB, Roberts DA, Tague CL, Jones C, Quattrochi DA, McFadden JP. Remote sensing and energy balance modeling of urban climate variability across a semi-arid megacity. Urban Clim. 2021 Jan;35:100757.

25. Ganci G, Cappello A, Bilotta G, Del Negro C. How the variety of satellite remote sensing data over volcanoes can assist hazard monitoring efforts: The 2011 eruption of Nabro volcano. Remote Sens Environ. 2020 Jan;236:111426.

26. Fu X, Yao L, Xu W, Wang Y, Sun S. Exploring the multitemporal surface urban heat island effect and its driving relation in the Beijing-Tianjin-Hebei urban agglomeration. Appl Geogr. 2022 Jul;144:102714.

27. Chanchí Golondrino GE, Ospina Alarcón MA, Saba M. Vegetation Identification in Hyperspectral Images Using Distance/Correlation Metrics. Atmosphere (Basel) [Internet]. 2023 Jul 14;14(7):1148. Available from: https://www.mdpi.com/2073-4433/14/7/1148

28. Saha D, Manickavasagan A. Machine learning techniques for analysis of hyperspectral images to determine quality of food products: A review. Curr Res Food Sci. 2021;4:28–44.

29. Spilsbury MJ, Euceda A. Transformada Rápida de Fourier. Rev la Esc Física. 2016;4(2):45–52.

30. Chanchí-Golondrino G-E, Ospina-Alarcón M-A, Saba M. Fourier Analysis Approach to Identify Water Bodies Through Hyperspectral Imagery. Rev Fac Ing [Internet]. 2023;33(67):e17232. Available from: https://revistas.uptc.edu.co/index.php/ingenieria/article/view/17232

doi: 10.25100/iyc.v26i3.13493